Vernier Microcombs for Integrated Optical Atomic Clocks

Kaiyi Wu[1*†], Nathan P. O'Malley[1†], Saleha Fatema[1], Cong Wang[1,3], Marcello Girardi[2], Mohammed S. Alshaykh[4], Zhichao Ye[2], Daniel E. Leaird[1,5], Minghao Qi[1], Victor Torres-Company[2] and Andrew M. Weiner[1]

[1]School of Electrical and Computer Engineering, Purdue University, West Lafayette, 47907, IN, USA.
[2]Department of Microtechnology and Nanoscience, Chalmers University of Technology, SE-41296, Sweden.
[3]Currently with Department of Surgery, University of Pittsburgh, 15219, PA, USA.
[4]Electrical Engineering Department, King Saud University, Riyadh, 11421, Saudi Arabia.
[5]Currently with Torch Technologies, supporting AFRL/RW, Eglin Air Force Base, FL, USA.

*Corresponding author(s). E-mail(s): wu1871@purdue.edu;
†These authors contributed equally to this work.

1 Deriving Frequency Division Effect with Only Two Microcomb Locks

As a result of the phase locks on f_{xCEO} and f_{Vernier}, the repetition rates of the two microcombs are stabilized at the level of the optical reference. This results in a frequency division effect, as explained in the following. The clock frequency can be expressed in terms of the two microcomb beats being phase-locked (f_{xCEO} and f_{Vernier}) to the LO laser using Eqs. 1, 2, & 5:

$$f_{\text{clock}} = \frac{1}{17292}(f_{871} - 2f_{\text{xCEO}} + 385f_{\text{Vernier}}). \tag{S1}$$

$f_{871} \sim 344$ THz is an optical frequency, while the other two beats for locking are at the GHz level ($f_{\text{Vernier}} \sim -8$ GHz and $f_{\text{xCEO}} \sim 20.4$ GHz). f_{871}

is roughly 4 and 2 orders of magnitude higher than $2f_{\text{xCEO}}$ and $385f_{\text{Vernier}}$, respectively. Importantly, in this work, the fiber comb optical reference and all RF references for the phase locks are stabilized to the same OCXO to eliminate relative drifting. Presuming good phase lock performance, such that the stability of the OCXO is transferred to the locked optical signals, the three terms on the right side of Eq. 11 will have similar fractional frequency instabilities. Given the multiple orders-of-magnitude differences in frequency of the terms in Eq. 11 and assuming good phase locks (hence similar fractional frequency instability), the clock output stability should be dominated by the stability of the optical frequency of the fiber comb-referenced LO laser. That is, $\Delta f_{\text{clock}}(t) \approx \Delta f_{871}(t)/17292$, where $\Delta f(t)$ denotes frequency fluctuations in time of f, in Hz. In reality the phase locks may not function ideally but will simply need to be good enough not to corrupt the frequency instability too badly (by two orders of magnitude, in the case of f_{Vernier}, and less stringent for the other lock). Note that if the Vernier beat frequency can be tuned closer to zero, the contribution of the Vernier term to the frequency instability of the clock will be reduced accordingly. In principle, the synchronizing signal for the phase locks here derived from the OCXO could instead be derived from the RF clock output. This would allow referencing of these locks to an atomic reference in an actual optical atomic clock system.

We can further consider the third phase lock ($f_{\text{LO}-\text{FC}}$) using Eqs. 6 and 11:

$$f_{\text{clock}} = \frac{1}{17292}(f_{\text{FC}} + f_{\text{LO}-\text{FC}} - 2f_{\text{xCEO}} + 385f_{\text{Vernier}}), \tag{S2}$$

which reveals the requirements for locking the 871 nm laser to the fiber comb by a similar line of reasoning. Since $f_{\text{LO}-\text{FC}}$ is roughly five orders of magnitude lower than the 344 THz LO, this is the least demanding of the three locks.

In summary, we expect frequency division from optical-to-RF with only a small contribution from the phase locks, even despite the free-running f_{CEO}.

2 Estimating Optical Stability of Fiber Comb Modes

As we are using one of the fiber comb lines as the optical reference, in this section we estimate its frequency instability. The frequency instability of any given fiber comb mode can be straightforwardly seen through the typical frequency comb equation ($f_m = m \times f_{\text{rep}} + f_{\text{CEO}}$) to depend on the two terms $m \times f_{\text{rep}}$ and f_{CEO}. In lieu of measuring the actual optical stability of a comb mode directly (which would require a second stable optical reference not available in our laboratory), one can measure the stability of each of the two terms separately to form an optical stability estimate. The fractional frequency instability of the $m \times f_{\text{rep}}$ term can be easily obtained by measuring the repetition rate at 250 MHz, as described in the main text. The fractional instability of $m \times f_{\text{rep}}$ should then ideally be the same as f_{rep}. The stability of the f_{CEO} term is estimated by sending an in-loop monitor output of the fiber comb offset

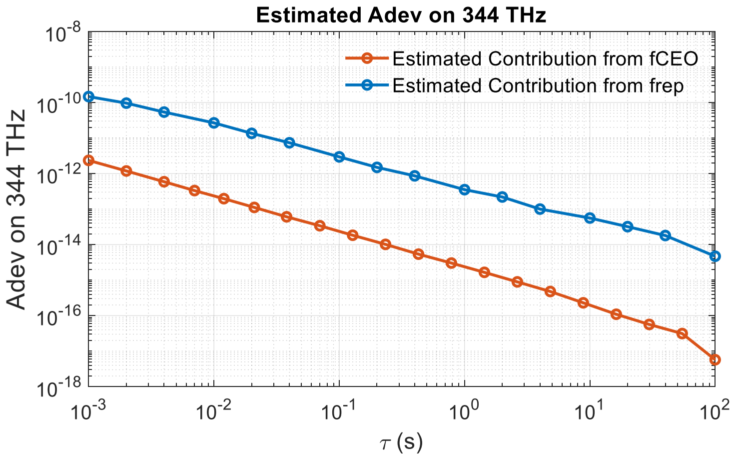

Fig. S1 Estimated relative contributions of the repetition rate and CEO frequency to the 344 THz optical reference line.

frequency to a frequency counter referenced to the GPS-disciplined oscillator. The resulting frequency instabilities from the two measurements can be seen in figure S1, clearly indicating that the repetition rate contribution is expected to dominate the CEO frequency contribution. Thus we estimate the optical mode's fractional frequency instability simply as that of the repetition rate.

3 Interferometric noise investigation

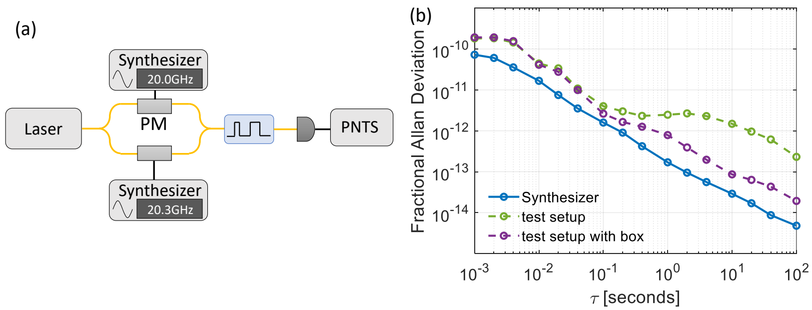

Fig. S2 Investigation on the interferometric noise using an analogous test setup. **a**, the schematic of the test setup. **b**, Fractional Allan deviations of the heterodyne beat between the first sidebands generated by two phase modulators with (purple line) and without (green line) a cover, and the frequency reference (blue line).

To gain insight into the interferometric noise in our system, we investigate a simple fiber interferometer setup with a stable heterodyne beat frequency as shown in Fig. S2a, analogous to our dual-comb configuration as a proof-of-concept experiment. Here we place a phase modulator (analogous to the microring) in each arm of a fiber Mach-Zehnder interferometer. The two phase modulators are driven by two synthesizers at 20 GHz and 20.3 GHz, respectively. We optically filter the first sideband from both arms and measure the frequency stability of the heterodyne beat note (analogous to the clock beat in the microcomb system). The two synthesizers are synchronized to a common 10 MHz clock, so in absence of optically-introduced noise, we expect this signal to be quite frequency-stable, and average down as $\sim 1/\tau$. However, we again observe a plateau feature in the Allan deviation in this measurement, closely resembling the plateau feature in the clock in the dual-microcomb system discussed in the main text (see Fig. S2b). This experiment indicates that the plateau feature of our clock signal is due to fiber-related noise in the interferometer-like segment of our microcomb system. To mitigate the environmental effects, we cover the interferometer setup in Fig. S2a with a foam box, which can block most of the airflow in the laboratory. The Allan deviation improves significantly and no longer shows an obvious plateau feature, although there is still excess frequency noise (Fig. S2b).

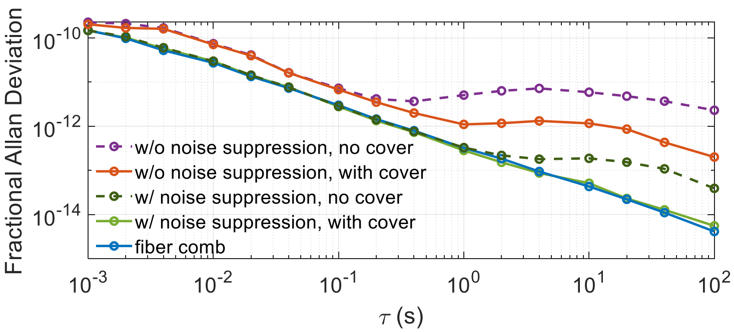

Fig. S3 Fractional Allan deviations of the clock output without and with the effects of noise-suppression scheme and the covers, and the fiber comb optical reference.

We also further investigate the interferometric noise effects in the dual-comb setup and attempt to estimate the noise suppression ratio achieved. Figure S3 shows the measured clock instabilities with and without foam partitions covering the setup and with and without noise suppression. The orange and green solid curves are the instabilities with the foam covers in place, without and with our noise suppression scheme, respectively, as reported in the main text. Without noise suppression, there is excess frequency instability at short averaging times and a plateau starting around 1 s average time. With noise suppression, the fractional frequency instability is brought down to that of the optical reference, which constitutes our measurement floor. The difference between the orange and green solid curves suggests $\sim$30-40$\times$ improvement; however, since we reach our measurement floor, this estimate is a lower bound. To gain additional information, we remove part of the foam cover and again compare the fractional frequency instability without and with noise suppression (purple and green dashed lines, respectively). This raises the noise further above that of the optical reference and provides an increased dynamic range for measurement. Here we estimate 40× noise suppression in the plateau region. A simple theoretical estimate of our noise suppression scheme (see the last section of Supplementary) based on the slight wavelength difference between the participating comb lines for $f_{\mathrm{clock}+}$&$f_{\mathrm{clock}-}$ suggests that ideally, the noise suppression capability should be of the same order of magnitude but somewhat higher. The difference may arise from noise or nonlinearities in our electronic mixing and division scheme.

4 Frequency Counter Resolution Limitations

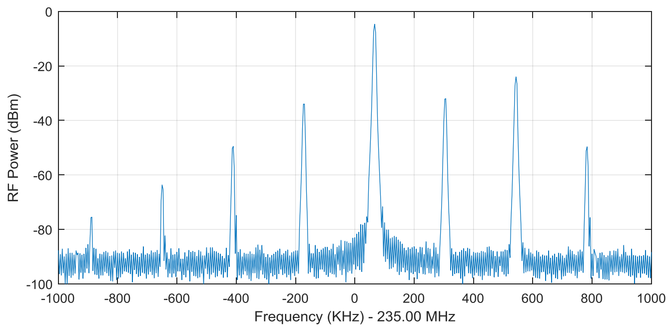

Fig. S4 Electrical spectrum analyzer trace of noise-suppressed clock output at 3 kHz RBW.

As noted in the main text, Fig. 4e (the time trace of the noise-suppressed clock output) shows a wider trace width than is seen in Fig. 4d (the time trace of the 871 nm laser). We attribute this to resolution limitations of our frequency counters. In order to support our claim, we observe that, as mentioned in the main text, our noise-suppressed clock output is not a pure sinusoid. Due to the nonlinearity of the mixer combining $f_{\mathrm{clock}+}$ and $f_{\mathrm{clock}-}$, there are spurious tones in the output spectrum, as can be seen in Fig. S4. The spurs are separated by ∼240 kHz, as expected, due to the 40 MHz shift applied to $f_{\mathrm{clock}-}$ and the electrical division factor of 168. In addition to the typical counter timing jitter-related resolution limits, these spurious tones can cause extra noise in the frequency counter measurement.

We confirm this by testing one of our frequency counters with synthesized waveforms from an arbitrary waveform generator (AWG). Initially, a pure sinusoidal tone is generated at ∼235 MHz, the frequency of the noise-suppressed clock, and sent to the frequency counter at 100 ms gate time (driven by an external gate signal). The data are plotted in Fig. S5a (yellow trace). The resulting trace appears cleaner than the clock output (plotted here in the blue

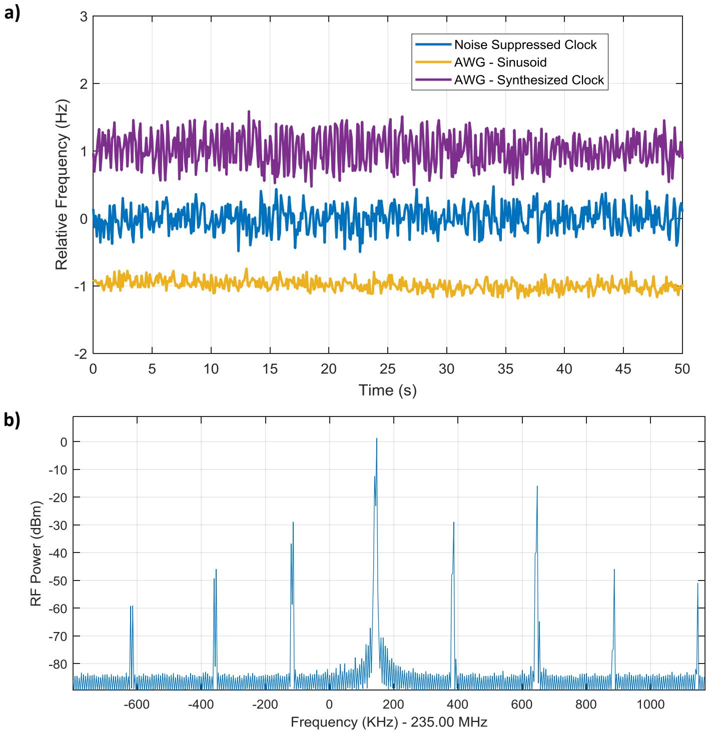

Fig. S5 **a**, counter measurements of the ∼235 MHz noise suppressed clock signal (blue trace), ∼235 MHz sinusoid generated by AWG (yellow trace), and the AWG-synthesized clock signal (purple trace). **b**, Electrical spectrum analyzer trace of AWG-synthesized clock signal at 1 kHz RBW.

trace for comparison) and is approximately at the resolution limit of the frequency counter. Note the traces have been shifted in post-processing for easier comparison. The AWG is then programmed to generate a waveform with a spectrum nearly identical to that of the clock (see Fig. S5b), and the counter trace becomes noisier as a result (purple trace). This effect is observed with a flat phase on each tone in the spectrum, as well as in two further trials with randomized phases applied to each line when programming the AWG (not shown here). This indicates the additional spectral content increases noise in the frequency counter measurement.

In summary, in addition to noise introduced by the clock being near the timing jitter-induced resolution limit of the frequency counter, the spurious signals in the noise-suppressed clock (caused by nonlinearities in our electronic mixer) induce further degradation in the counter measurement of the clock. We attribute the differences between Figs. 4d and e to these causes.

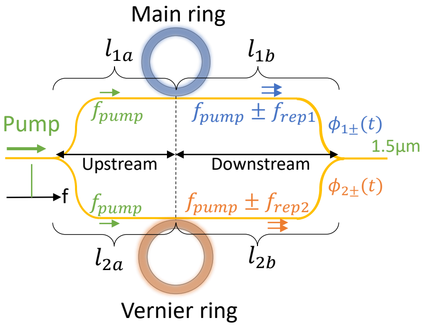

Fig. S6 Schematic illustration of the dual-comb setup notated with physical parameters.

5 Theoretical analysis of noise suppression

We theoretically analyze the effectiveness of our noise suppression scheme with the participating comb lines for $f_{\text{clock}+}\&f_{\text{clock}-}$ being at slightly different frequencies. Fig. S6 shows a simplified dual-comb schematic notated with the physical parameters involved in the analysis. $l_{1\text{a}}$ and $l_{2\text{a}}$ denote the fiber lengths between the splitting of the pump and the main and Vernier microrings, respectively. $l_{1\text{b}}$ and $l_{2\text{b}}$ denote the fiber lengths from the main and Vernier rings to where the fibers are combined. We assume the phase fluctuations in the fibers result from fiber length variations, and the refractive index n for the participating comb lines in the fibers remain constant for simplification in the analysis. The fiber length with phase fluctuations can thus be written as follows:

$$l_{\text{x}}(t) = \bar{l}_{\text{x}} + \delta l_{\text{x}}(t) \tag{S3}$$

which consists of the average value $\bar{l}_{\text{x}}$ that is constant in time, and the time varying length $\delta l_{\text{x}}(t)$ contributed by the fiber noise. The subscript x denotes 1a, 2a, 1b, 2b, the four segments of the fiber length of interest.

The phase fluctuation $\phi(t)$ for the participating comb lines of $f_{\text{clock}+}$ and $f_{\text{clock}-}$ can be expressed in terms of fiber length:

$$\begin{aligned}
\phi_{1+}(t) &= \frac{2\pi f_{\text{pump}} n}{c} l_{1\text{a}}(t) + \frac{2\pi (f_{\text{pump}} + f_{\text{rep1}}) n}{c} l_{1\text{b}}(t), \\
\phi_{1-}(t) &= \frac{2\pi f_{\text{pump}} n}{c} l_{1\text{a}}(t) + \frac{2\pi (f_{\text{pump}} - f_{\text{rep1}}) n}{c} l_{1\text{b}}(t), \\
\phi_{2+}(t) &= \frac{2\pi f_{\text{pump}} n}{c} l_{2\text{a}}(t) + \frac{2\pi (f_{\text{pump}} + f_{\text{rep2}}) n}{c} l_{2\text{b}}(t), \\
\phi_{2-}(t) &= \frac{2\pi f_{\text{pump}} n}{c} l_{2\text{a}}(t) + \frac{2\pi (f_{\text{pump}} - f_{\text{rep2}}) n}{c} l_{2\text{b}}(t),
\end{aligned} \tag{S4}$$

where we use $\phi_{1+}(t)$ and $\phi_{2+}(t)$ for the higher-frequency sidebands for the main and Vernier comb line, respectively, and similarly, we use $\phi_{1-}(t)$ and $\phi_{2-}(t)$ for the lower-frequency sidebands.

For the noise-suppressed clock, we modify Eqs. 8 & 9 in the main text by considering the wavelength dependence of ϕ_1 and ϕ_2 using the above equations (Eq. S4) and obtain:

$$f_{\mathrm{clock}+} + f_{\mathrm{clock}-} = 2(f_{\mathrm{rep1}} - f_{\mathrm{rep2}}) + \frac{1}{2\pi}(\phi'_{1+} - \phi'_{2+} + \phi'_{2-} - \phi'_{1-}). \tag{S5}$$

Thus, the additional frequency instability under the noise suppression scheme is from the time-varying phase terms. Substituting the expressions of Eq. S4 into Eq. S5, we obtain the residual frequency noise for the noise-suppressed clock:

$$\begin{aligned}\delta(f_{\mathrm{clock}+} + f_{\mathrm{clock}-}) &= \frac{n}{c}[2f_{\mathrm{rep1}}\delta l'_{\mathrm{1b}}(t) - 2f_{\mathrm{rep2}}\delta l'_{\mathrm{2b}}(t)] \\ &\approx \frac{n}{c}2f_{\mathrm{rep}}[\delta l'_{\mathrm{1b}}(t) - \delta l'_{\mathrm{2b}}(t)].\end{aligned} \tag{S6}$$

$l'_{\mathrm{x}}(t)$ is the time derivative of $l_{\mathrm{x}}(t)$. The time derivative of phase fluctuation $\phi'(t)$ is from the fiber length fluctuation $l'_{\mathrm{x}}(t)$. Using the relation in Eq. S3 and since $\bar{l}_{\mathrm{x}}$ is constant, we have $l'_{\mathrm{x}}(t) = \delta l'_{\mathrm{x}}(t)$. Additionally, since the two microcomb repetition rates differ by only $\sim 2\%$, we approximate them as $f_{\mathrm{rep1}} \approx f_{\mathrm{rep2}} \approx f_{\mathrm{rep}}$.

The fractional frequency instability for the noise-suppressed clock is:

$$\frac{\delta(f_{\mathrm{clock}+} + f_{\mathrm{clock}-})}{2f_{\mathrm{clock}}} \approx \frac{n}{c}\frac{f_{\mathrm{rep}}}{f_{\mathrm{clock}}}[\delta l'_{\mathrm{1b}}(t) - \delta l'_{\mathrm{2b}}(t)]. \tag{S7}$$

This equation indicates that ideally the frequency noise remaining after the suppression scheme depends only on fiber length fluctuations downstream from the microrings; in the ideal case length fluctuations experienced by the pump upstream from the microrings cancel out completely. Note that care is needed in interpreting the subtraction operation on the right hand side of eq. S7. If the length fluctuations are highly correlated and in phase, they will tend to cancel each other out. However, if the length correlations are uncorrelated, their effects add incoherently.

For comparison, we also deduce the fiber-related frequency noise without the noise suppression. The clock without noise suppression can be written as:

$$f_{\mathrm{clock}+} = f_{\mathrm{rep1}} - f_{\mathrm{rep2}} + \frac{1}{2\pi}(\phi'_{1+} - \phi'_{2+}). \tag{S8}$$

The fiber-related frequency noise will be:

$$\begin{aligned}\delta f_{\mathrm{clock}+} &= \frac{n}{c}f_{\mathrm{pump}}(\delta l'_{\mathrm{1a}} - \delta l'_{\mathrm{2a}}) + \frac{n}{c}[(f_{\mathrm{pump}} + f_{\mathrm{rep1}})\delta l'_{\mathrm{1b}} - (f_{\mathrm{pump}} + f_{\mathrm{rep2}})\delta l'_{\mathrm{2b}}] \\ &\approx \frac{n}{c}f_{\mathrm{pump}}(\delta l'_{\mathrm{1a}} - \delta l'_{\mathrm{2a}} + \delta l'_{\mathrm{1b}} - \delta l'_{\mathrm{2b}}).\end{aligned} \tag{S9}$$

Since the repetition rate is only 0.5% of the pump frequency, in the second line of Eq. S9 we consider the sideband frequencies approximately equal to the pump frequency. In this approximation $\delta f_{\text{clock}-} \approx \delta f_{\text{clock}+}$. We thus use δf_{clock} to represent either clock signal interchangeably. The fiber-related frequency noise for f_{clock} depends on the pump frequency and the phase fluctuation both upstream and downstream of the microrings. Using $l_{\text{j}} = l_{\text{ja}} + l_{\text{jb}}$ and $\delta l'_{\text{j}} = \delta l'_{\text{ja}} + \delta l'_{\text{jb}}$ (j = 1,2), we can express the fractional frequency instability as:

$$\frac{\delta f_{\text{clock}}}{f_{\text{clock}}} \approx \frac{n}{c}\frac{f_{\text{pump}}}{f_{\text{clock}}}(\delta l'_1 - \delta l'_2). \tag{S10}$$

To characterize the effectiveness of the noise-suppression scheme, we define a parameter η equal to the ratio of the fractional frequency instability without (Eq. S10) and with (Eq. S7) noise-suppression.

$$\eta = \frac{f_{\text{pump}}}{f_{\text{rep}}}\frac{\delta l'_1 - \delta l'_2}{\delta l'_{1\text{b}} - \delta l'_{2\text{b}}} = \eta_f \eta_l. \tag{S11}$$

Thus, in theory, the noise-suppression ratio is the product of two factors. The first is the frequency-dependent term $\eta_f = f_{\text{pump}}/f_{\text{rep}}$, which is $\sim$200 in our experiment. The second factor η_l depends on the time-dependent fiber length fluctuations, including the correlations (or lack of correlations) between them. The behavior of η_l depends on the specific experimental layout and environment perturbations.